JOURNAL OF SPACECRAFT AND ROCKETS
Vol. 39, No. 3, May–June 2002

Plasma Propulsion Options for Multiple Terrestrial Planet Finder Architectures

Kurt A. Polzin,* Edgar Y. Choueiri,† Pini Gurfil,‡ and N. Jeremy Kasdin§
Princeton University, Princeton, New Jersey 08544

A systems-level trade study is presented comparing the propulsion requirements and associated final masses for different architectural implementations of the Terrestrial Planet Finder mission. The study focuses on the millinewton-level propulsion chores associated with rotating and repointing an array. Three interferometer configurations, free flying, monolithic, and tethered, lead to estimates of thrust and power requirements and spacecraft masses associated with the different plasma propulsion systems required to perform maneuvers throughout a mission. The parametric study includes the following plasma propulsion options: Hall thruster, field emission electric propulsion, ablative pulsed plasma thruster, ablative Z-pinch pulsed plasma thruster, and gas-fed pulsed plasma thruster. Not all of the thrusters considered can perform the necessary propulsive chores for each architecture, but for the most promising thruster and architecture combinations, it is found that the initial mass for a system falls between 3050 and 4060 kg. The tether, in general, possesses the lowest initial mass of the three architectures followed by the free flyer and the monolith. Finally, the thrust-to-power ratio, maximum deliverable thrust or impulse bit, and capability of a propulsion system to process enough power to produce a required thrust level are shown to be more important factors than the specific impulse in determining the proper thruster choice for moderate to high thrust maneuvers.

Nomenclature

a	=	square side length, m
g_0	=	Earth's gravitational acceleration, m/s^2
H	=	angular momentum, kg · m^2/s
I	=	moment of inertia, kg · m^2
$I_{\text{bit max}}$	=	maximum deliverable impulse bit, mN · s
I_{coll}	=	collector I, kg · m^2
I_{comb}	=	combiner I, kg · m^2
I_{sp}	=	specific impulse, s
I_{truss}	=	monolith truss I, kg · m^2
I_1	=	tether retracted I, kg · m^2
M	=	moment applied to spacecraft, N · m
m	=	mass, kg
m_{coll}	=	collector mass, kg
m_{comb}	=	combiner mass, kg
m_f	=	final (propellantless) mass, kg
m_{fixed}	=	fixed mass excluding propulsion, kg
m_i	=	initial (total) mass, kg
$m_{p\text{(fixed)}}$	=	fixed power supply mass, kg
m_{pay}	=	payload mass, kg
m_{PPU}	=	power processing unit (PPU) mass, kg
m_{prop}	=	propellant mass, kg
m_{ps}	=	total power supply mass, kg
$m_{\text{ps(thr)}}$	=	thruster power supply mass, kg
m_{solar}	=	mass of solar arrays, kg
m_{tank}	=	tankage mass, kg
$m_{\text{thr(fixed)}}$	=	fixed thruster mass, kg
m_{truss}	=	monolith truss mass, kg
P_{fixed}	=	constant (fixed) power required, W
P_{max}	=	maximum required power, W
P_{min}	=	minimum required power, W
P_{solar}	=	power provided by solar array, W
P_{thr}	=	thruster required power, W
P_{total}	=	total required power, W
R	=	outer radius, m
R_{coll}	=	collector R, m
R_{comb}	=	combiner R, m
R_{truss}	=	monolith truss R, m
T_{max}	=	maximum deliverable thrust, mN
T_{req}	=	required thrust, mN
T/P	=	thrust-to-power ratio, mN/W
t_{extend}	=	tether extension time, s
t_m	=	mission length, s
t_{retract}	=	tether retraction time, s
t_{rot}	=	rotational period, s
x, y	=	lateral spacecraft dimensions, m
α	=	specific mass, kg/kW
α_a	=	average angular acceleration, rad/s^2
Δt	=	time for a maneuver, s
Δv	=	characteristic mission velocity, m/s
$\Delta\theta$	=	repointing angle, rad
η_{PPU}	=	PPU efficiency
η_t	=	thruster efficiency
ω	=	rotational velocity, rad/s
ω_1	=	tether retracted ω, rad/s

Received 24 July 2001; revision received 16 January 2002; accepted for publication 16 January 2002.

*National Defense Science and Engineering Graduate Fellow, Electric Propulsion and Plasma Dynamics Laboratory, Applied Physics Group, Mechanical and Aerospace Engineering Department, Engineering Quadrangle, Olden Street. Member AIAA.

†Chief Scientist, Electric Propulsion and Plasma Dynamics Laboratory and Assistant Professor, Applied Physics Group, Mechanical and Aerospace Engineering Department, Engineering Quadrangle, Olden Street. Associate Fellow AIAA.

‡Postdoctoral Researcher, Dynamics and Control Group, Mechanical and Aerospace Engineering Department, Engineering Quadrangle, Olden Street.

§Assistant Professor, Dynamics and Control Group, Mechanical and Aerospace Engineering Department, Engineering Quadrangle, Olden Street.

Introduction

THE motivation behind this work is NASA's Terrestrial Planet Finder (TPF) mission.[1] TPF is a cornerstone project in NASA's Origins program to look for planets capable of supporting life outside the solar system. One imaging approach being considered is the use of a nulling interferometer to block out starlight, thus allowing a companion planet to be more easily seen. An implementation being considered would have TPF using multiple, free-flying spacecraft to perform several different missions over its lifetime including planet finding, medium depth spectroscopy, deep spectroscopy, and astrophysics.[1]

In this paper, we examine only the primary mission objective, planet finding. Three possible configurations for the interferometer

are considered: 1) a free-flying formation of spacecraft, 2) a monolithic assembly over a deployable truss, and 3) a tethered constellation. In all three cases, we assume that there are four collectors and a single combiner used as a sparse aperture rotating interferometer. Note that the monolith and tethered configurations, both considered as structurally connected, may not be able to perform all of the tasks that a free flyer could perform due to their more limited degrees of freedom.

A previous study by Stephenson[2] examined tradeoffs in metrics of initial mass, mission adaptability, and mission capability for two interferometer configurations, free flying and monolithic. That study did not, however, take into account the variable mass of the power supply required to operate a plasma propulsion system. It also did not explore changes to the metrics that might arise from choosing a plasma propulsion option with different characteristic performance values.

We focus here on the tradeoffs between the propellant mass savings and the power mass penalties associated with the use of a plasma propulsion system over three distinct interferometer configurations. In addition to varying the configuration, we also vary the type of plasma propulsion system to represent a wide range of available performance characteristics. The problem is examined taking into account systems aspects, specifically power usage and power supply sizing. We also consider the power and mass savings due to a consolidation of redundant subsystems in the structurally connected architectures. It will be shown that by approaching the problem in this way interesting conclusions can be reached regarding the reasonable choices one could make to complete this mission.

The Δv and thrusting requirements computed for each architecture are only for the millinewton-level tasks performed during planet finding and not the micronewton-level tasks that would be needed for fine positioning of an interferometer. However, it can be assumed that, because thrusters currently under development for micronewton-level propulsion tasks are lightweight and consume very little power,[3] their inclusion would not greatly impact our results. A recent paper[4] focused on evaluating thrusters for micronewton-level propulsion tasks.

The TPF mission is performed in deep space,[1] and as such, the values of Δv calculated are relative to a reference point in space, located at the rotational center of the interferometer. This rotational center moves through space in an heliocentric orbital trajectory. The Δv required for the system to reach this orbital trajectory is not included in this study. From a propulsion point of view, planet finding is the worst-case scenario when using free flyers in that more propellant, thrust, and power are needed than for the spectroscopic or astrophysics missions. For the purposes of this study, we will assume this worst-case mission to occupy the entire five-year lifetime of TPF. The propulsion systems considered are 1) Hall thrusters, 2) field emission electric propulsion (FEEP), 3) ablative pulsed plasma thrusters (APPT), 4) ablative Z-pinch pulsed plasma thrusters (AZPPT), and 5) gas-fed pulsed plasma thrusters (GF-PPT). A recent general description of these types of systems may be found in Ref. 5.

A discussion on how the spacecraft power requirements and mass are broken down is presented and includes the methods used to size the power supply and reference data on the performance of all of the thrusters considered in this study. Then, the mission involving the free-flying interferometer is explored. Here, two different free-flying scenarios will be described, and the mass, power, and Δv tradeoffs for each propulsion system in this architecture will be discussed. Next, the tradeoffs associated with the use of a monolithic interferometer configuration to complete a comparable reference mission are studied. A tethered interferometer is then studied as a third alternative. Finally, a head-to-head comparison of each of the propulsion system/configuration combination is made highlighting the strengths and weaknesses of each.

Power, Mass, and Propulsion

Spacecraft Power

The power requirements can be split into two basic parts, where the total power required is the sum of the power required to 1) operate the spacecraft's instruments and perform housekeeping tasks and 2) operate the thruster, P_{thr}. Under the assumption that power needs for task 1 are constant, the power requirements scale with P_{thr}. We find P_{thr} by taking the maximum required thrust during the mission and dividing it by a given thruster's characteristic thrust-to-power ratio T/P.

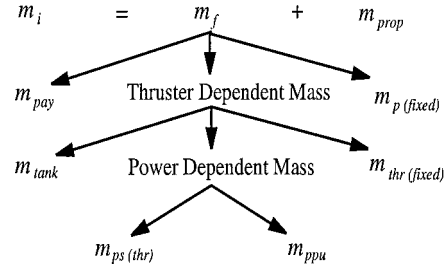

Fig. 1 Typical mass breakdown for a plasma propulsion system.

Spacecraft Mass

As shown in Fig. 1, the initial (total) spacecraft mass m_i is made up of a final mass m_f and a propellant mass m_{prop}. The propellant mass is itself also a function of the final mass through the rocket equation. The final spacecraft mass is divided into three general parts: payload mass m_{pay}, mass of the equipment required to power the spacecraft's instruments and perform housekeeping tasks $m_{p(\text{fixed})}$, and mass contributions for the hardware needed to operate the thruster. When the thruster contribution is broken down even further, there is a tankage mass associated with propellant storage and feeding m_{tank}, a fixed hardware mass associated with each thruster $m_{\text{thr(fixed)}}$, and a power-dependent thruster mass associated with the generation of power for the thruster. Finally, the power-dependent thruster mass is divided into two terms. The first is the mass of the power supply $m_{\text{ps (thr)}}$, which contains all of the hardware necessary to generate power for thruster operation (batteries, solar cells, etc.). The second is the mass of the power processing unit (PPU), m_{PPU}, which is the mass of any equipment needed to take the power provided by the spacecraft bus and adapt it to meet a specific thruster's voltage and current requirements.

Power Supply

Two major components of the power system are kept variable and sized to provide the appropriate level of power for spacecraft operation. These variable components are the solar arrays (J. M. Troutman, Integrated Design Solutions, LLC, Lawrenceville, NJ, personal communication, Oct. 2001) and a battery storage system.

Solar Array

The solar cells adopted in the present study are of the multijunction gallium arsenide type, the performance of which has been extensively characterized, and not the concentrator array-type solar panels recently demonstrated on Deep Space 1 (Ref. 6). The individual solar cells are assumed to have an area of 24.3 cm^2 and a specific mass of 3.1 kg/m^2 and are sized using a method (Troutman, personal communication, 2001) to scale the array voltage and power output to the desired levels. The number of cells in series is selected so that the maximum power output by one string corresponds to an unregulated (sunlight regulated) voltage of 36 V. Included in this number are the diode and harness voltage drops up to the main bus distribution point. The number of parallel strings in the array are then chosen to scale the maximum power output to the desired level. Based on the number of cells in series and parallel strings and the specific mass, the overall area and mass of an array can be calculated. However, there is a practical limit to the size of the solar array one could use, which we assume to be 8 m^2. This estimate falls in the middle of the range of sizes for solar arrays found on currently orbiting satellites.[7–9] To fully address the issue of maximum solar array size, however, the structural issues of the array itself and the systems issues regarding the space available for stowing the array during launch would have to be taken into account. These issues are beyond the scope of this paper.

Battery

The battery type we assume for this mission is based on small cell lithium-ion battery technology.[10] Each cell can provide 5.4 W · h of power storage capacity at a specific mass of 40.5 g/cell plus a 25% parasitic mass (S. Martins, COM DEV Battery Products, Cambridge, ON, Canada, personal communication, Oct. 2001). Like the solar arrays, the battery is constructed in a modular fashion by combining cells in series to form strings and strings in parallel to meet the power storage requirements. To get an output of 28 V to the spacecraft bus requires a string of six cells in series, and these strings provide 32.4 W · h each. Note that the battery voltage is less than the solar array operating voltage, as it must be to fully charge the battery (Troutman, personal communication, 2001). In this study, each cell in the battery will discharge and recharge at a rate of 5.4 W (1-C or rated level). Although the battery could discharge and recharge at a faster rate, this will affect its lifetime by lessening the amount of power the battery can store throughout the duration of the mission. A ground test conducted under low Earth orbit LEO conditions is currently underway for this type of battery and has achieved 40,000 cycles discharging/recharging at the 1.8-C level (1.8 × 5.4 W/cell) (Martins, personal communication, 2001).

We assume that there is a battery on each spacecraft capable of a minimum power storage of 100 W · h. For cases where the power consumption history has short periods of high power usage between long periods of low power usage and P_{max}, which is the maximum power usage level, is greater than P_{solar}, which is the power level the solar array can provide (Fig. 2a), batteries must be employed to make up the difference during peak usage periods. In these cases, the solar array is sized to provide P_{min} and recharge the battery between peak usage periods. The battery is then sized to provide, in conjunction with the solar array, the power level P_{max} during peak usage periods. Battery recharging time should not impact the number of observations that can be made over the mission life as long as the time integral of excess power provided by the solar arrays during the low power usage periods is greater than the time integral of the excess power required from the batteries during peak usage. If the recharging time for a specific case requires more time than we allow, we will consider this to be, within our assumptions, a limitation of the thruster/architecture combination being discussed.

For cases where the power consumption history is essentially constant throughout the mission (Fig. 2b), the solar array is simply sized to provide this constant level of power. In these cases, the battery would simply have the minimum capacity of 100 W · h, but would not be used during the idealized mission (either discharged or recharged) because all of the necessary power for spacecraft operation could be provided by the solar array.

Propulsion Systems

Table 1 contains a list of the relevant operating parameters for each plasma thruster used in this paper. The thrusters are the Hall thruster, FEEP, APPT, AZPPT, and GF-PPT. Descriptions and background on each of these devices may be found in Refs. 5 and 11–16. Note that the APPT used in this study is an electromagnetic version with performance characteristics approximating the current state-of-the-art EO-1 PPT.[14] An electrothermal APPT is being developed by Rysanek and Burton,[17] but its performance characteristics are not used here because they are similar to those of the AZPPT.[15]

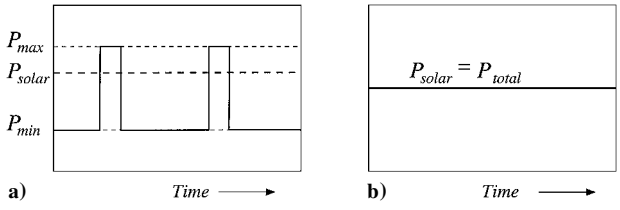

Fig. 2 Typical power consumption histories (solid line) for a spacecraft firing its thrusters a) at regular intervals several hours apart or b) continuously.

The fixed mass per thruster for the all PPTs are 0.75 kg, whereas the module (mainly capacitor) mass is 2.30 kg (W. A. Hoskins, General Dynamics, Redmond, WA, personal communication, Nov. 2001). One PPT module is used for every three thrusters. The mass of the housing for a solid-propellant (ablative) PPT is taken to be 40% of the propellant mass (Hoskins, personal communication, 2001), whereas the tankage mass for the GF-PPT is 60% of the propellant mass.[18] Hall thrusters will use the same tankage mass fraction as the GF-PPT with a fixed thruster mass of 0.75 kg. For FEEP, the thruster assembly and neutralizer cathode have a mass of 0.5 kg/thruster,[19] and there is no tankage mass fraction because the thruster assembly is also the propellant reservoir. The mass of the PPU is handled by multiplying the amount of power required by the PPU specific mass, α, which is a technology-dependent characteristic parameter for any given thruster. PPU efficiencies are not included in η_t and do need to be taken into account because α should be multiplied by the total power delivered to the propulsion system by the spacecraft bus.

PPTs use a flyback-converter-type PPU to charge the capacitor to a high voltage before it is discharged. These PPUs have efficiencies of ~80% and can process up to 120 W of power, but they do not scale well to higher powers (Hoskins, personal communication, 2001) due to high voltage arcing in the electronics. In our analysis, if more than 120 W of total thruster power is required, multiple PPUs, thrusters, and modules are added to the spacecraft. PPTs are most limited in the total impulse they can deliver by their capacitor life, which is about 2×10^7 pulses.[14] Although we take the limitation on the amount of power a PPT PPU can process to be the more stringent constraint, the cases where the capacitor lifetime would be exceeded before the mission is completed will still be noted in the course of our analysis.

Hall thruster PPUs produce high current levels at relatively low voltages with an efficiency of ~90% (Hoskins, personal communication, 2001), whereas PPUs for electrostatic thrusters (FEEP) produce high voltages at low currents with an efficiency of 92% (Ref. 6). Both systems can process kilowatts of power at a time. The lifetime of both these thrusters, however, is limited by the lifetime of the cathode emitter. Cathode life tests have been demonstrated to 28,000 h (Ref. 20) and 32,000 ignition cycles[21] have been achieved.

The Hall thruster generally leads in technology readiness (as long as operation is maintained above 500 W), followed by the ablative PPT options, then FEEP, and finally the GF-PPT. Hall thrusters have been used in orbit for many years[22] and are scheduled to be used as a primary propulsion system on the ESA-sponsored SMART-1 technology demonstrator.[23] However, Hall thrusters operating at levels below 500 W are not available and are currently in the research phase of development.[24,25] APPTs were first flight qualified in the 1970s.[26] They have flown on the NOVA satellites in the 1980s[27] and have recently been flown on the EO-1 spacecraft.[14] AZPPTs would presumably use relatively similar flight hardware to that found in current APPTs. Cesium propellant FEEP thrusters have not been flight qualified to date, but they may be close to achieving that milestone.[28] Indium propellant FEEP, however, has been flown on several missions over the past 10 years.[29] Both FEEP thruster options

Table 1 Summary of characteristics for different plasma propulsion systems

System	Propellant	I_{sp}, s	$I_{bit\,max}$	T_{max}, mN	T/P, μN/W	η_t, %	η_{PPU}, %	$\propto$, kg/kW
Hall[5,11]	Xe	1,600	——	80	60	50	90	7
FEEP[11,12]	Cs	10,000	——	5	16	80–100	92	10
APPT[11,13,14]	Teflon	1,000	297 μN · s	——	15	7	80	5
AZPPT[15]	Teflon	650	2 mN · s	——	30	2–9	80	5
GF-PPT[16]	Xe, Ar	7,000	40 μN · s	——	7	2–13	80	5

Table 2 Matrix of the different advantages/disadvantages of each propulsion system

System	Pros	Cons
Hall	Moderate I_{sp} and high T/P give rise to reasonable propellant mass and power requirements. Space-proven technology. Low plume contamination risk.	Higher fixed mass and complexity due to tankage and valves. Presently limited to operation above 500 W. Low-power Hall thruster not yet ready.
FEEP	High I_{sp} leads to low propellant mass. Low overall system mass. Indium thruster tested in space.	Low T/P gives rise to high power requirements. High α leads to heavy PPU. Thruster lifetime unknown. Cesium thruster untested in space. Contamination by plume. More thrust required in some cases than current FEEP systems can provide.
APPT	Moderate I_{sp} and T/P give rise to reasonable propellant mass and power requirements. Space-proven technology. System simplicity and reliability.	Higher fixed mass due to capacitor. Contamination by Teflon plume. PPU limited in amount of power it can process.
AZPPT	High T/P gives rise to reasonable power requirements. Space-proven technology. System simplicity and reliability.	Low I_{sp} leads to high propellant mass. Higher fixed mass due to capacitor. Contamination by Teflon plume. PPU limited in amount of power it can process.
GF-PPT	High I_{sp} leads to low propellant mass. Low plume contamination risk.	Low T/P gives rise to high power requirements. Higher fixed mass and complexity due to tankage and capacitor. PPU limited in amount of power it can process.

Table 3 Free flyer fixed mass and power levels excluding those associated with propulsion (after Ref. 1)

Parameter	Outer collector	Inner collector	Combiner
m_{fixed}, kg	644	643	605
P_{fixed}, W	325	325	865

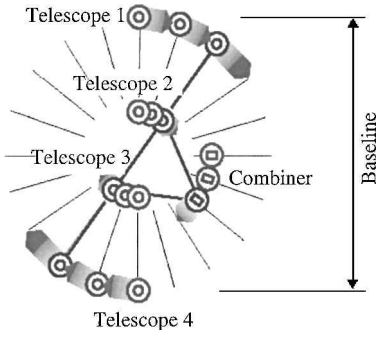

Fig. 3 Flight path during planet finding for a free-flying interferometer following a circular path (from Ref. 1).

are in competition for use on NASA's LISA mission[30] and ESA's infrared space interferometry (IRSI-DARWIN) mission,[28] both of which are scheduled to precede TPF. To date, a flight prototype GF-PPT system has been constructed[31,32] but has not yet been flight qualified.

Cesium FEEP systems present the highest potential for spacecraft and optics contamination, followed by Teflon® propellant ablative PPTs and indium propellant FEEP systems. The Hall thruster and GF-PPT, both of which can operate with inert gases, present the least problem from a spacecraft and optics contamination standpoint. Presented in Table 2 is a matrix of the advantages and disadvantages of the various propulsion options as they relate to this mission.

Free-Flying Interferometer

The first mission examined is that consisting of several free-flying spacecraft moving in formation to form a sparse-aperture array. The fixed masses associated with each spacecraft and the power requirements excluding those for the propulsion system are taken from Ref. 1. There are five spacecraft: two outer collectors, two inner collectors, and a combiner. The masses and power requirements are given in Table 3.

Different types of closed-path revolutions have been previously studied.[2] In that work, two different scenarios for the free flyer are developed.

In the first scenario (Fig. 3), the outer and inner collectors and the combiner revolve in a circle around some fixed point relative to the system with the collectors remaining in a straight line for the entire revolution. While on this flight path, the spacecraft must fire their thrusters continuously at a low-thrust level to keep on their respective circular paths.

The total Δv needed to complete one closed circular path is given by the formula[2]

$$\Delta v_c = 4\pi^2 R/t_{rot} \tag{1}$$

The total Δv for the mission is then

$$\Delta v_{c\,total} = \frac{4\pi^2 R t_{mis}}{t_{rot}^2} \tag{2}$$

where t_{mis} is taken in this study as five years. The mass of each spacecraft is given by the rocket equation as

$$m_i = m_f \exp\left(\frac{\Delta v_{c\,total}}{I_{sp} g_0}\right) \tag{3}$$

with the mass of the propellant being the difference between m_i and m_f. The required thrust needed to provide the centripetal acceleration is

$$T_{req} = m_i \omega^2 R = m_i (2\pi/t_{rot})^2 R \tag{4}$$

Finally, the power needed for propulsion and the mass of the power processing unit are

$$P_{thr} = \frac{T_{req}}{T/P}, \qquad m_{PPU} = \frac{\alpha P_{thr}}{\eta_{PPU}} \tag{5}$$

A second scenario developed by Stephenson[2] was that of a closed flight path consisting of a square instead of a circle. In this scenario, the spacecraft follow square paths equal in perimeter to the circular path. Unlike the circular path, the spacecraft thrusters fire only at the corners of the square path giving the spacecraft long stretches of flight unperturbed by thruster operations.

For a square path with perimeter and rotational period that are equal to those of a circular path of radius R, the Δv required for one rotational period is[2]

$$\Delta v_s = \sqrt{2} \cdot 4^2 a \Big/ t_{rot}$$

$$= \sqrt{2} \cdot 4 \Delta v_c a \Big/ (\pi^2 R) \tag{6}$$

where a is 106 m for a 135-m baseline. This equation assumes that the change in Δv occurs nearly instantaneously (when compared to the period of rotation) and that the thrust vector forms an angle of 135 deg with both the incoming and outgoing velocity vectors located at a corner of the square. The total Δv for the mission lifetime is then

$$\Delta v_{s\,\text{total}} = \sqrt{2} \cdot 4^2 a t_{\text{mis}} \Big/ t_{\text{rot}}^2$$

$$= \sqrt{2} \cdot 4(\Delta v_{c\,\text{total}}) a \Big/ (\pi^2 R) \tag{7}$$

The mass fraction is again given by Eq. (3). We assume that, to change the spacecraft direction at the corners of their paths, the thrusters fire for 10% of the total rotational period. The necessary thrust in this case is given by the relation

$$T_{\text{req}} = m_i \Delta v_s / (0.1 t_{\text{rot}}) \tag{8}$$

where the numerator is the total impulse needed for the completion of one rotational period. Propulsive power requirements and PPU masses are still obtained from Eq. (5). The possible motivations for using a square path as opposed to a circular one are twofold. First, a reduction in the Δv requirement for each spacecraft per revolution can be realized, potentially translating into a reduced propellant mass. Second, perturbations in the spacecraft excited by thruster operation will not be present during the observation period, which could translate into a greater attainable precision in the relative positioning of the spacecraft in the array.

For planet finding, the spacecraft could follow the perimeter of any n-sided polygon ($n \geq 4$ and even to maintain symmetry in the interferometer). The cases of $n = 4$ (a square) and $n \to \infty$ (a circle) give upper and lower bounds on the thrust and Δv requirements assuming that the fraction of the rotational period during which the thruster operates rises with n (from 10% for $n = 4$ to 100% for $n \to \infty$).

As mentioned earlier, we are only concerned in the present study with the millinewton-level thrust needed to rotate the array about some reference point. Left out are the micronewton-level thrusters that will surely be needed to finely position the individual free flyers in the array while maintaining the tight tolerances required for interferometry. Although the additional mass of these thrusters and their power requirements are not an issue for larger spacecraft such as those being proposed for TPF, these issues would need to be considered if much smaller spacecraft were used for a formation flying mission.

One way to repoint a free-flying array is to simply perform a fraction of the planet finding maneuver, rotating the array about its center until it was pointed at a new target star. Stephenson stated[2] that the repointing of the array can be neglected because the associated Δv is a small fraction of that needed to constrain the array baseline during an observation. However, our assumption that planet finding is performed throughout the operational lifetime of the array (the worst-case scenario from a Δv standpoint) overestimates the total Δv requirement. Although, strictly speaking, we neglect repointing in the our calculations, the overestimated Δv can be thought of as containing repointing maneuvers.

Representative Mission

For the free flyer, we assume planet finding is performed continuously for the entire mission lifetime as opposed to the shorter time frame being considered for the free-flyer mission.[1] This assumption may, in some cases, bias the results in favor of higher I_{sp} devices. However, the structurally connected architectures, especially the monolithic truss, will be more difficult to reconfigure once on station and may not be capable of performing the other tasks currently being considered for the free-flying architecture. By restricting the mission to planet finding, we allow for a fair comparison to be made between the different architectures.

Whereas the thrusters operate over the entire rotational period for the case of a circular path, they only fire over 10% of the rotational period for the square path when the spacecraft reaches a corner. We assume[1] an observation period of 8 h and a baseline of 135 m. This baseline is for the circular flight path, with the square flight path having an equal perimeter.

Results and Discussion

In this section, the important calculated parameters for the free-flyer mission are presented for each spacecraft in the five-spacecraft array using each of the five thrusters cited in Table 1. The parameters of interest are found in Table 4 for each spacecraft following the circular flight path and in Table 5 for the square flight path.

The Δv requirement is, as expected, lower for the square-path case when compared to that of the circular path by about 10%. Also, the difference in the initial masses for the circular-path case are within about 7%. There is some I_{sp} induced bias in these initial masses due to the assumption that planet finding is performed throughout the mission. Even so, this bias is, in general, a small effect because the required Δv is relatively low when compared to the characteristic values of I_{sp} for the various propulsion options.

The Δv advantage gained by using a square-path, however, is largely negated due to the higher thrust and associated power required along the square path. The spacecraft thrust and power requirements, as well as the number of propulsive units needed to produce the necessary thrust, have at least as large an effect on the initial mass as the I_{sp} induced bias. In the case of PPTs (especially the GF-PPT and the APPT) their low T/P leads to thruster power levels that can only be processed by multiple PPT units. As is seen in Table 5, these requirements can become prohibitively large for some propulsive options.

In both cases, 5475 observations can be performed (neglecting repointing time), whereas the total impulse required is $\sim 3.5 \times 10^5$ N·s for the outer collectors and $\sim 1 \times 10^5$ N·s for the inner collectors and combiner. For the PPTs, roughly 10^8 pulses are required over the course of the mission for the circular path to deliver this much total impulse, which is about an order of magnitude higher than current capacitor lifetimes. The thrust levels are much higher in the square-path case because roughly the same impulse must be delivered in $\frac{1}{10}$th the time. The higher thrust levels,

Table 4 Calculated parameters for free-flying spacecraft following a circular flight path and using different plasma propulsion systems

Parameter	Hall	FEEP	APPT	AZPPT	GF-PPT
			Outer collector		
Thruster sets required	1	1	2	1	4
P_{thr}, W	40	145	195	100	405
P_{total}, W	365	470	520	425	730
m_{solar}, kg	5	7	7	6	10
m_{ps}, kg	6	8	9	7	11
m_{prop}, kg	22	4	36	57	5
m_i, kg	690	660	725	740	705
Δv, m/s	507	507	507	507	507
			Inner collector		
Thruster sets required	1	1	1	1	2
P_{thr}, W	14	45	60	30	130
P_{total}, W	340	370	385	355	455
m_{solar}, kg	5	5	5	5	6
m_{ps}, kg	6	6	7	6	8
m_{prop}, kg	7	1	12	18	2
m_i, kg	665	655	675	685	675
Δv, m/s	169	169	169	169	169
			Combiner		
Thruster sets required	1	1	2	1	2
P_{thr}, W	15	45	60	30	125
P_{total}, W	880	910	925	895	990
m_{solar}, kg	12	13	13	13	14
m_{ps}, kg	14	14	25	14	15
m_{prop}, kg	7	1	8	17	2
m_i, kg	640	625	668	655	640
Δv, m/s	169	169	169	169	169
			Total		
P_{total}, W	2290	2590	2735	2455	3360
m_i, kg	3340	3250	3440	3500	3390

Table 5 Calculated parameters for free-flying spacecraft following a square flight path and using different plasma propulsion systems

Parameter	Hall	FEEP	APPT	AZPPT	GF-PPT
			Outer collector		
Thruster sets required	1	4	19	9	55
P_{thr}, W	370	1370	2215	1000	6530
P_{min}, W	325	325	325	325	325
P_{max}, W	695	1695	2540	1325	6855
m_{solar}, kg	10	24	25	19	25
m_{ps}, kg	11	25	32	20	73
m_{prop}, kg	20	3.3	42	58	8.5
m_i, kg	695	700	920	830	1265
Δv, m/s	456	456	456	456	456
			Inner collector		
Thruster sets required	1	2	5	3	12
P_{thr}, W	120	435	580	280	1355
P_{min}, W	325	325	325	325	325
P_{max}, W	445	760	905	605	1680
m_{solar}, kg	6	11	13	8.5	24
m_{ps}, kg	7.5	12	14	10	25
m_{prop}, kg	6.5	1	11	16.5	1.8
m_i, kg	665	665	720	705	785
Δv, m/s	152	152	152	152	152
			Combiner		
Thruster sets required	1	2	5	3	11
P_{thr}, W	115	415	555	270	1280
P_{min}, W	865	865	865	865	865
P_{max}, W	980	1280	1420	1135	2145
m_{solar}, kg	14	18	20	16	25
m_{ps}, kg	15	19	21	17	29
m_{prop}, kg	6	1	11	16	2
m_i, kg	635	635	690	675	745
Δv, m/s	152	152	152	152	152
			Total		
P_{max}, W	3260	6190	8310	4995	19215
m_i, kg	3355	3365	3970	3745	4845

whereas not greatly affecting the Hall thruster or FEEP options, require many more PPT modules on each spacecraft. A beneficial side effect, though, of having many PPT modules on each spacecraft is that each capacitor has to provide only $\sim 10^7$ pulses, which is an achievable number.

The FEEP option following a circular flight path has the lowest initial mass of all free-flying configuration cases. FEEP performing the square-path mission has an initial mass that is ~4% higher than FEEP on the circular path. The Hall thruster option has about the same initial mass for each path, allowing for the versatility to follow both circular and square flight paths during the same mission. Using any type of PPT to follow a circular flight path increases the initial mass of the interferometer by at most 8% over the Hall thruster and FEEP options. The initial mass becomes prohibitively large for PPT options when traveling on a square flight path, with a minimum mass increase over the Hall thruster and FEEP options of 11.5%.

The free-flying interferometer architecture ranks low from a maturity standpoint; however, EO-1 has successfully demonstrated formation flying as a viable technology.[33] Free-flying architectures are currently being considered for both the IRSI-DARWIN[28] and LISA[30] missions. Flight experience on either of these missions would serve to increase the maturity of the free-flying architecture before a TPF mission launch.

Monolithic Interferometer

The spacecraft in a free-flying architecture depend on the propulsion system to constrain their motions to closed flight paths. A monolithic architecture, on the other hand, has all its components physically connected by a truss. As such, once a monolithic interferometer is on station, the only propulsive requirements are spinning the array up in speed and repointing it.

The Δv to spinup or spindown the array is given by

$$\Delta v_{spin} = \omega R = 2\pi R / t_{rot} \tag{9}$$

where R has been taken to be the radius of the outer collectors for a conservative estimate. The moment needed to accomplish this maneuver is

$$M = I\alpha_a = I\omega/\Delta t = 2\pi I/(t_{rot}\Delta t) \tag{10}$$

When it is assumed that the collectors are lumped masses m_j (lumped at their center of mass and located at a distance R_j from the center of the monolith) and that the combiner and connecting trusses have some finite dimension and a roughly uniform mass distribution, the moment of inertia is given by

$$I = \sum I_{coll} + \sum I_{truss} + I_{comb} \tag{11}$$

where each component's moment of inertia is given by

$$I_{coll} = m_{coll} R_{coll}^2$$

$$I_{truss} = m_{truss} R_{truss}^2 + m_{truss}\left(x_{truss}^2 + y_{truss}^2\right)/12$$

$$I_{comb} = m_{comb}\left(x_{comb}^2 + y_{comb}^2\right)/12 \tag{12}$$

In Eqs. (12), R_{coll} is the radius from the rotational center of the array, m_{truss} is the mass of a truss that has its center located a distance R_{truss} from the rotational center and has cross-sectional dimensions x_{truss} and y_{truss}, and m_{comb}, x_{comb}, and y_{comb} are the combiner's mass and cross-sectional dimensions, respectively. There are thrusters firing symmetrically about the axis of rotation, and the required thrust for each side of the array is

$$T_{req} = M/(2R) \tag{13}$$

where R is the outer radius of the array.

There are two possible ways to repoint the array. The first is to spin down the array to rest, rotate it about a different axis until it is pointed at a new target system, and then spin up the array to the observation speed again. The values of Δv for both spinning down and spinning up the array are given by Eq. (9). The Δv for repointing the array is given as

$$\Delta v_{repoint} = 2\omega_{max} R \tag{14}$$

where ω_{max} is the maximum rotational velocity achieved during the repointing. Furthermore, ω_{max} occurs at $\Delta\theta/2$ and $\Delta t/2$, which are half the total repointing angle and time, respectively. Using this in the appropriate equations of motion and rearranging yields

$$\Delta v_{repoint} = 4\Delta\theta R/\Delta t \tag{15}$$

The necessary moment to repoint can be found by integrating the equation of motion $M = I\ddot{\theta}$ with the appropriate boundary conditions and evaluating at $\omega = \omega_{max}$. This moment is

$$M = 4I\Delta\theta/\Delta t^2 \tag{16}$$

The required thrust for each side of the array is still given by Eq. (13). The total Δv for the entire monolith mission using this type of repointing maneuver can be written as

$$\Delta v_{total} = (2\Delta v_{spin} + \Delta v_{repoint})(t_m/t_{tot})$$

$$t_{tot} = 2t_{spin} + t_{rot} + \Delta t \tag{17}$$

where t_{spin} is the time to spin up or spin down the array.

A second way to repoint the array is to precess it about an axis while it is still spinning. The angular momentum H is related to the applied moment by

$$M = \frac{dH}{dt} \tag{18}$$

where $H = I\omega$ and ω is the rotational velocity of the array. When the change in angular momentum due to repointing is written as $\Delta H = I\omega\Delta\theta$, where $\Delta\theta$ is the repointing angle, Eq. (18) can be written as

$$M = 2T_{req}R = \Delta H/\Delta t = I\omega\Delta\theta/\Delta t \tag{19}$$

When Newton's second law is used, $F\,\mathrm{d}t = \mathrm{d}(mv)$, where m is assumed to remain constant during the maneuver and T_{req} is substituted for F, Eq. (19) can be rewritten as

$$T_{\mathrm{req}}\Delta t/m = \Delta v_{\mathrm{precess}} = I\omega\Delta\theta/(2Rm) \tag{20}$$

where Δt is now the time for precessing the array. Finally, the moment needed to accomplish this maneuver is

$$M = I\omega\Delta\theta/\Delta t \tag{21}$$

As before, the required thrust is given by Eq. (13). The total Δv for an entire monolith mission where repointing is accomplished through precession is

$$\Delta v_{\mathrm{total}} = \Delta v_{\mathrm{spin}} + \Delta v_{\mathrm{precess}}(t_m/t_{\mathrm{tot}}), \qquad t_{\mathrm{tot}} = t_{\mathrm{rot}} + \Delta t \tag{22}$$

Repointing can be accomplished by either method 1 (spin down, repoint, spin up) or method 2 (precessing). To maximize the number of observations performed over the course of the mission, we choose to minimize the repointing time by employing method 2. The spacecraft mass is calculated through Eq. (3), and as in the free-flyer configuration case, the total PPU mass and power required by the thruster are given by Eq. (5).

Representative Mission

The assumptions we make are meant to illustrate the differences between the monolithic and free-flying architectures. Figure 4 shows that there are five separate optical components in the monolithic architecture, just like in the free-flying array, two outer collectors, two inner collectors, and a combiner, except they are now connected by rigid trusses. The mass and power requirements for each component are essentially the same as for each analogous component in the free-flying architecture; however, we do assume some consolidation in the attitude control, communications, and data management systems. Whereas each free-flying spacecraft requires a complete set of these systems, only one set of each system is needed when the array is structurally connected because control commands can be carried through cables from a single control center to any component in the array. The payload masses of the collector and combiner modules are 593 and 605 kg, respectively with corresponding fixed power requirements of 186 and 865 W. Also, thrusters and PPU systems are only required on the outer collectors for spinning up and repointing the array, with five thrusters per set located on each end for full control. All of the required power systems are to be located at the combiner, with power distributed through cables running along the truss to the collectors.

The outer truss sections are taken at roughly 45 m in length and are calculated, following Stephenson,[2] to have a mass of 68 kg each, whereas the inner ones are half the length and mass. The combined mass estimate for a truss and deployment mechanism, as cited by Stephenson,[2] is 988 kg. We subtract the truss section masses from this number to find the mass of the deployment mechanism. This mass is assumed to vary linearly with truss length and is divided into three equal parts and added into the masses of the combiner and the two inner collector modules. For moment of inertia calculations, the trusses are taken to have a square cross section of 0.75 m, and the combiner is taken to be roughly a 2×2 m box. Both are assumed to have a uniform mass distribution.

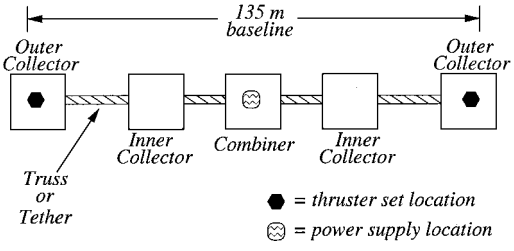

Fig. 4 Configuration of the fully extended structurally connected interferometers assumed for this study.

Table 6 Calculated parameters for a monolithic interferometer using different plasma propulsion systems

Parameter	Hall	FEEP	APPT	AZPPT	GF-PPT
			Outer collector		
Thruster sets required	1	1	2	1	4
P_{thr}, W	45	160	200	100	435
m_{prop}, kg	1	$\mathcal{O}$(100 g)	1	2	$\mathcal{O}$(100 g)
			Combiner		
m_{solar}, kg	24	25	25	25	25
m_{ps}, kg	25	27	27	26	32
			Total		
Δv, m/s	5.5	5.5	5.5	5.5	5.6
P_{min}, W	1610	1610	1610	1610	1610
P_{max}, W	1700	1930	2010	1810	2480
m_i, kg	4000	4000	4030	4010	4060

The observation period is maintained at 8 h with observations taking place over the entire five-year mission of the interferometer. The monolith performs one spin-up maneuver at the beginning of its mission and then performs a repointing maneuver after each observation. A repointing maneuver takes 30 min to complete and is performed over an angle of $\pi/8$ rad. The repointing Δv is very sensitive to the repointing angle, whereas the moment [and through Eq. (13) the thrust] is sensitive to the ratio of $\Delta\theta/\Delta t$. The repointing angle and time chosen here are relatively arbitrary and could be the subject of a separate optimization study. However, in this study they serve to illustrate the tradeoffs in required thrust and power between architectures and plasma propulsion options.

Results and Discussion

Several calculated parameters for the monolithic architecture are presented in Table 6. The Δv is low relative to the free-flying array because the motion of each component in the array is passively constrained by the truss and not through active thrusting. Also, the required thrust is low because it is applied over a long moment arm.

For this architecture, 5150 observations can be performed. This is fewer than the number for the free flyer, but the time to repoint the free-flying array was neglected. Including the repointing time might similarly impact the number of observations the free-flying architecture can perform. The total impulse needed is $\sim 4 \times 10^4$ N · s. This is an order of magnitude less than the impulse required for the free-flying interferometer.

The low required thrust and Δv translate into an m_{prop}, m_{ps}, and m_i that are all relatively insensitive to the propulsion option selected. Note that I_{sp} induced biasing of the initial mass is not an issue here because the characteristic values of I_{sp} for the various propulsive options are much greater than the required Δv. The variation of m_i over all options is only $\sim$1.5%. However, even with the mass savings due to the low Δv requirement and subsystem consolidation, the mass penalty due to the truss and deployment mechanism are large and make this architecture, in general, the most massive.

The best thruster options for use with this architecture are the Hall thruster, FEEP, and the AZPPT. APPT or GF-PPT require a number of pulses greater than 2×10^7 to deliver the total required impulse, implying lifetime is an issue for these options.

The monolithic truss architecture in this study is the simplest and most mature from a construction and control standpoint. It is, however, the most massive and least adaptable and reconfigurable once it is on station. Last, for the free flyer, the inner collectors' optimum thrust vectors are directed toward the outer collectors, increasing the chances of spacecraft/plume interaction and contamination. In the monolith architecture, because the structure, and not the thrusters, constrain the rotational motion, no thrusters are required to fire through any components. As such, spacecraft/plume contamination should be reduced for the monolith architecture.

Tethered Interferometer

As in the case of the monolithic architecture, the tethered interferometer's components are all physically connected. The assumptions of subsystem consolidation presented for the monolith

are maintained for the present case because power and command signals can be distributed to each spacecraft in the array from a central point through the tether. A small mass is added to the payload mass of the combiner (assumed to be 20 kg) and inner collectors (assumed to be 10 kg each) to account for the mechanism for extending/retracting the tether.[34] Extension/retraction units, most notably the Small Expendable Deployment System (SEDS), have had some initial validation in space.[35]

For the analysis, we assume that the tethered system represents a rigid body,[36] much like the monolith. The system spins up as a single body with all tethers retracted and all spacecraft rigidly connected. The rigid connections then disengage, and the tethers extend to the observation length. The assumption that the tethered spacecraft behave like a rigid body is only possible if the tethers are extended and retracted slowly enough to allow line vibrations to be damped.[36,37] Damping can be accomplished using thrusters, offset control, and tension control.[37,38] As the tethers extend, the outer spacecraft slow down due to their increasing moment of inertia and exert a force through the tether on the inner spacecraft, which slows them down as well. The entire system gradually slows in a manner similar to that of a rigid body, with its total moment of inertia increasing with extension. Once an observation is complete, the tethers retract (again, slow enough to maintain the rigid-body assumption). The spacecraft engage their rigid connections and repoint by precession. The tethers are retracted to give the ability to control more easily the individual spacecraft during the precession maneuver.

Though the problem of controlling the extension/retraction of a spinning, linear tethered system has not yet been solved, the problem has been solved for a spinning, triangular array[36] and a nonspinning, linear array.[37] Because the TPF mission will be performed in deep space, perturbations due to the gravitational gradient, which are large for tethered systems in Earth orbit, should be negligible.

During spin up, the retracted system must attain a much higher rotational speed compared to the observational speed. The spin-up speed is determined by applying conservation of angular momentum and is given by

$$\omega_1 = \omega I / I_1 = 2\pi I / (t_{\text{rot}} I_1) \tag{23}$$

where ω and I are the rotational speed and the moment of inertia of the extended system and ω_1 and I_1 are the rotational speed and the moment of inertia of the retracted system, respectively. The calculation of I is the same as for the monolith given in Eqs. (11) and (12) except there is no truss and, therefore, no I_{truss}. The calculation of I_1 cannot assume that any of the spacecraft are point masses while the tethers are retracted. The retracted tether moment of inertia is given by

$$I_1 = \sum_j I_{1j}, \qquad I_{1j} = \frac{m_j\left(x_j^2 + y_j^2\right)}{12} + m_j R_j^2 \tag{24}$$

where the summation is over the five spacecraft in the array.

The formulas for calculating Δv and the moments required for both spin up and repointing are the same as those in the monolith section, except I and ω are replaced by I_1 and ω_1. The total Δv for the entire mission is given by Eq. (22), but additional terms accounting for the time to extend and retract the tethers must be included in t_{tot}, which is now written as

$$t_{\text{tot}} = t_{\text{rot}} + \Delta t + t_{\text{extend}} + t_{\text{retract}} \tag{25}$$

Representative Mission

The assumptions here are similar to those for the monolith with one important exception. For obvious controllability reasons, it is easier to repoint the system at a new target star if the tethers are retracted and all five spacecraft are rigidly connected to one another. Therefore, we assume that, between observations, the tethers are retracted from the baseline of 135 m (Fig. 4) to a more compact size, which decreases the total moment of inertia and increases the rotational velocity. The system performs a repointing maneuver by precessing about its rotational axis and reextends the tethered components, decelerating to the observation speed. The same cross-sectional dimensions as the monolith's combiner (2×2 m) are used here for all five spacecraft.

We assume a spinup time of 30 min. Each repointing maneuver is performed over 30 min and an angle of $\pi/8$ rad, as in the monolith case. The time to extend or retract the tethers is taken to be 30 min, that is, 1 h total per repointing maneuver.[37,38]

Results and Discussion

The summary of calculated parameters for the tethered configuration case is presented in Table 7. The payload masses for the outer and inner collectors and combiner are 593, 603, and 625 kg, respectively. The fixed power requirements for this configuration are the same as those of the monolith case.

The Δv required for this case is an order of magnitude larger than that required for the monolith and an order of magnitude smaller than that required for the free-flying array. The difference in the values of Δv for monolithic and tethered architectures is due to its inverse scaling with the radius from the rotational center to the thruster location as shown in Eq. (20).

The tethered architecture performs ~4600 observations. This is fewer than with both the monolithic and free-flying architectures due to the added time to retract and extend the tethers. The necessary total impulse is roughly 4×10^5 N · s, which is an order of magnitude more than in the case of the monolith and on the same order as the maximum total impulse for spacecraft in the free-flying architecture. The GF-PPT and APPT options must provide many more than 2×10^7 pulses to deliver the required total impulse for the tethered architecture, meaning capacitor lifetime is again an issue.

The tethered array requires more total power and thrust than either the monolithic array or the free-flying spacecraft following a circular path, but less than the free flyers following a square path. The total initial mass for the tethered architecture is, for the reasonable choices of the Hall thruster and FEEP options and the distant third-place choice of the AZPPT, lower than for any other architecture. For these choices, m_i varies by 14%, but if the AZPPT option is excluded, it only varies by ~1.5%. This architecture has many of the advantages of the monolithic array, chiefly lower Δv requirements and the opportunity to consolidate redundant subsystems, while eliminating the major disadvantage of the monolith, the heavy truss and deployment system.

This mission could be performed using Hall thrusters or a bank of multiple FEEP systems. The number of thruster units required for the PPT options (especially the APPT and GF-PPT) are prohibitively large due to both the low level of power a single unit can process and PPT's low T/P. All propulsive options except the Hall thruster require fairly substantial batteries to provide the necessary power

Table 7 Calculated parameters for a tethered interferometer using different plasma propulsion systems

Parameter	Hall	FEEP	APPT	AZPPT	GF-PPT
			Outer collector		
Thruster sets required	1	5	22	10	69
P_{thr}, W	450	1700	2360	1165	8270
m_{prop}, kg	7	1	14	18	3
			Combiner		
m_{solar}, kg	24.8	24.8	24.8	24.8	24.8
m_{ps}, kg	32	55	72.8	45	178.5
			Total		
Δv, m/s	67	67	76	72	88
P_{min}, W	1610	1610	1610	1610	1610
P_{max}, W	2510	5000	6330	3940	18150
m_i, kg	3045	3095	3480	3250	4400

Table 8 Matrix showing total initial mass for each architecture and thruster combination

	Mass m_i (kg)				
Architecture	Hall	FEEP	APPT	AZPPT	GF-PPT
Free flyer (circle)	**3340**	**3250**	**3440**	**3500**	**3390**
Free flyer (square)	**3355**	**3365**	3970	3745	4845
Monolith	**4000**	**4000**	**4030**	**4010**	**4060**
Tether	**3045**	**3095**	3480	**3250**	4400

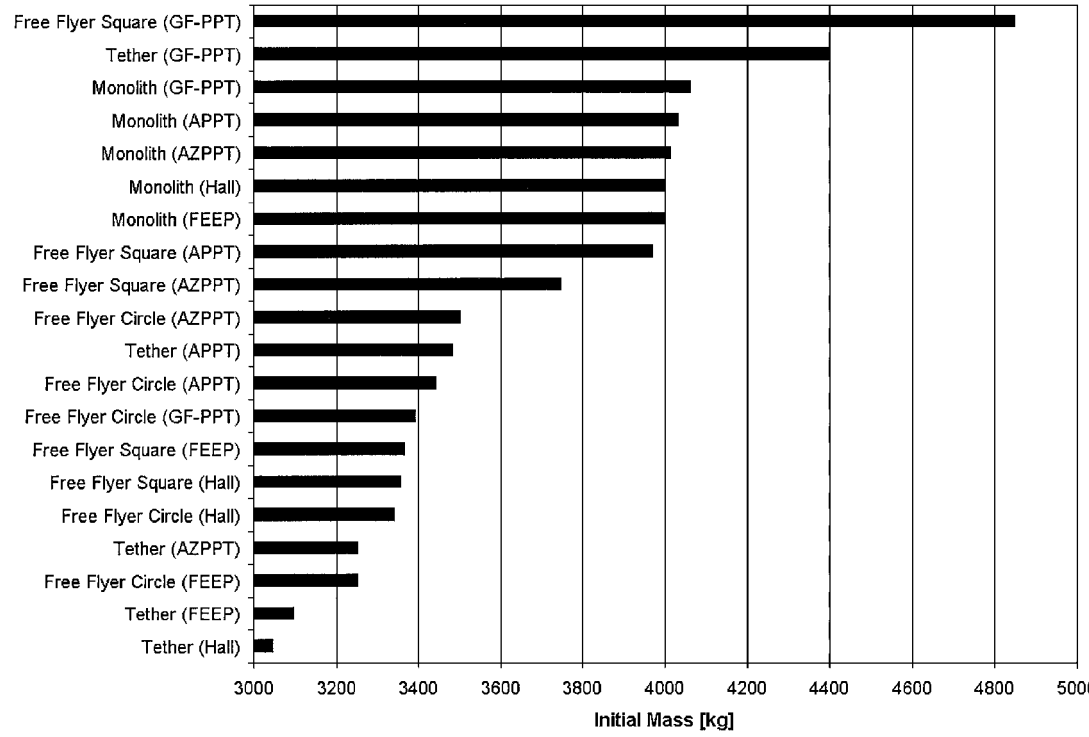

Fig. 5 Stackup of the initial masses m_i for each architecture and thruster combination.

during the repointing maneuver. The power required for the GF-PPT, APPT, and FEEP options is great enough that there is not enough time between maneuvers to recharge the batteries fully at the 1-C level (5.4 W · h/cell) as we assumed at the beginning of this study. Using these thruster options would limit the number of observations that could be made because the spacecraft would have to wait longer between repointing maneuvers to fully recharge its batteries.

Tethers have flown in the past as part of deployment and retrieval experiments. Detailed reviews of their development status, failure modes, and control issues are available in Refs. 39–42. As in the monolith case, the advantage of decreased spacecraft/plume interaction exists for this structurally connected configuration. Thrusters located on the outer collectors give full array controllability because the tethered system can be considered as a rigid body.

An overall comparison is made in Table 8 and Fig. 5 between all of the thruster/architecture combinations discussed in this paper. In Table 8, the numbers that are bold faced are the reasonable thruster options within each architecture. These choices exclude PPT capacitor lifetime issues.

Conclusions

This study leads to the following conclusions:

1) For the assumptions made and for reasonable propulsion options, the initial masses of each architecture fall within the range of 3050–4060 kg.

2) For promising propulsion options, the tethered architecture is generally the lowest in initial mass, followed by the free-flying and monolithic architectures. The difference between the mass of the free flyers and that of the monolithic structure is driven by estimates of the truss mass and deployment system. Past studies[1,2] had not considered any other structurally connected architectures other than the monolithic truss. Our inclusion of tethered spacecraft, with their lower associated structural mass, leads us to conclude that structurally connected architectures can possess initial masses that are lower than free flyers due to the free-flying architecture's larger Δv and propellant mass requirements.

3) The millinewton-level propulsion tasks, within the assumptions of this study, can be conducted only by certain thrusters. For the free flyer on a circular path and the monolith, all five thruster options are available due to the low required thrusts, whereas for the free flyer following a square path and the tethered interferometer, only Hall thrusters, FEEP, and possibly the AZPPT options are available because much higher thrust levels are required.

4) A thruster option's T/P, maximum producible thrust or impulse bit, and ability to process enough power to yield the necessary thrust are, in general, more important factors when selecting a propulsion system than I_{sp} for moderate to high thrust maneuvers.

Although there is a wide spread of the initial masses between the architectures, the performance of the reasonable plasma propulsion options is not an important differentiating index within a given architecture. As such, measures of 1) thruster lifetime, 2) technology readiness (of both the thruster and architecture), and 3) potential for spacecraft contamination by the exhaust plume products are more important when choosing both the thruster and architecture for the TPF mission.

Acknowledgments

This work was performed for the Jet Propulsion Laboratory, California Institute of Technology, sponsored by NASA. We gratefully acknowledge many helpful discussions with J. Troutman of Integrated Design Solutions, LLC, Lawrenceville, New Jersey; W. A. Hoskins of General Dynamics, Redmond, Washington; S. Martins of COM DEV Battery Products, Cambridge, Ontario, Canada; and J. R. Arrell.

References

[1]Terrestrial Planet Finder Science Working Group, *Terrestrial Planet Finder*, edited by C. A. Beichman, N. J. Woolf, and C. A. Lindensmith, NASA Jet Propulsion Lab., JPL Publ. 99-003, California Inst. of Technology, Pasadena, CA, 1999.

[2]Stephenson, R. L., "Comparative System Trades Between Structurally Connected and Separated Spacecraft Interferometers of the Terrestrial Planet Finder Mission," M.S. Thesis, Dept. of Aeronautics and Astronautics, Massachusetts Inst. of Technology, Cambridge, MA, May 1998.

[3]Mueller, J., "Thruster Options for Microspacecraft: A Review and Evaluation of State-of-the-Art and Emerging Technologies," *Micropropulsion for Small Spacecraft*, edited by M. M. Micci and A. D. Ketsdever, Vol. 187, Progress in Astronautics and Aeronautics, AIAA, Reston, VA, 2000, pp. 45–137.

[4]Reichbach, J. G., Sedwick, R. J., and Martinez-Sanchez, M., "Micropropulsion System Selection for Precision Formation Flying Satellites," AIAA Paper 2001-3646, July 2001.

[5]Jahn, R. G., and Choueiri, E. Y., "Electric Propulsion," *Encyclopedia of Physical Science and Technology*, 3rd ed., Vol. 5, Academic Press, San Diego, CA, 2002, pp. 125–141.

[6]Rayman, M. D., Varghese, P., Lehman, D. H., and Livesay, L. L., "Results from the Deep Space 1 Technology Validation Mission," *Acta Astronautica*, Vol. 47, Nos. 2–9, 2000, pp. 475–487.

[7]Murphy, D. M., "The Scarlet Solar Array," *Deep Space 1 Technology Validation Reports*, NASA Jet Propulsion Lab., JPL Publ. 00-10, No. 10, California Inst. of Technology, Pasadena, CA, 2000, pp. 371–406.

[8]Vellinga, J. M., Craig, C. L., Giellis, R. T., Rasbach, C. E., Rogers, J. J., Thornton, M. G., Willcockson, W. H., Brownlee, D. E., and Atkins, K. L., "Environmental Design Considerations for STARDUST," *27th International Conference on Environmental Systems*, Society of Automotive Engineers, SAE TP 972278, July 1997.

[9]Irish, R., *Landsat 7 Science Data Users Handbook*, Landsat Project Science Office, NASA Goddard Space Flight Center, Greenbelt, MD, 1999, Chap. 2, URL: http://ltpwww.gsfc.nasa.gov/IAS/handbook/handbook_toc.html [cited 1 March 2002].

[10]Lizius, D., Cowles, P., Spurrett, R., and Thwaite, C., "Lithium-Ion Satellite Batteries Using Small Cells," *NASA Aerospace Battery Workshop*, NASA TR 20010083626, Huntsville, AL, Nov. 2000.

[11]Martinez-Sanchez, M., and Pollard, J. E., "Spacecraft Electric Propulsion: An Overview," *Journal of Propulsion and Power*, Vol. 14, No. 5, 1998, pp. 688–699.

[12]Marcuccio, S., Genovese, A., and Andrenucci, M., "Experimental Performance of Field Emission Microthrusters," *Journal of Propulsion and Power*, Vol. 14, No. 5, 1998, pp. 744–781.

[13]Turchi, P. J., and Burton, R. L., "Pulsed Plasma Thruster," *Journal of Propulsion and Power*, Vol. 14, No. 5, 1998, pp. 716–735.

[14]Benson, S. W., Arrington, L. A., Hoskins, W. A., and Meckel, N. J., "Development of a PPT for the EO-1 Spacecraft," AIAA Paper 99-2276, June 1999.

[15]Markusic, T. E., Polzin, K. A., Levine, J. Z., McLeavey, C. A., and Choueiri, E. Y., "Ablative Z-Pinch Pulsed Plasma Thruster," AIAA Paper 2000-3257, July 2000.

[16]Ziemer, J. K., and Choueiri, E. Y., "Scaling Laws for Electromagnetic Pulsed Plasma Thrusters," *Plasma Sources Science and Technology*, Vol. 10, No. 3, 2001, pp. 395–405.

[17]Rysanek, F., and Burton, R. L., "Effects of Geometry and Energy on a Coaxial Teflon Pulsed Plasma Thruster," AIAA Paper 2000-3429, July 2000.

[18]Jordan, I. J. E., Schultz, A. B., Hart, H. M., Bruhweiler, F., Hershey, J., and Fraquelli, D., "UMBRAS: Design of a Free-Flying Occulter for Space Telescopes," AIAA Paper 2000-5230, Sept. 2000.

[19]Marcuccio, S., Genovese, A., and Andrenucci, M., "FEEP Microthruster Technology Status and Potential Applications," International Astronautical Federation, IAF Paper 97-S.3.04, 1997.

[20]Sarver-Verhey, T. R., "28,000 Hour Xenon Hollow Cathode Life Test Results," International Electric Propulsion Conf., IEPC Paper 97-168, Electric Rocket Propulsion Society, Santa Fe, NM, 1997, pp. 1030–1037.

[21]Zakany, J. S., and Piñero, L. R., "Space Station Cathode Ignition Test Status at 32,000 Cycles," International Electric Propulsion Conf., IEPC Paper 97-167, Electric Rocket Propulsion Society, Santa Fe, NM, 1997, pp. 1022–1029.

[22]Myers, R. M., "Overview of Major U.S. Industrial Programs in Electric Propulsion," AIAA Paper 2000-3147, July 2000.

[23]Snyder, J. S., "Propulsion and Energy: Electric Propulsion," *Aerospace America*, Vol. 38, No. 12, 2000, pp. 48–49.

[24]Khayms, V., and Martinez-Sanchez, M., "Design of a Miniaturized Hall Thruster for Microsatellites," AIAA Paper 96-3291, July 1996.

[25]Raitses, Y., and Fisch, N. J., "Parametric Investigation of Non-Conventional Hall Thruster," *Physics of Plasmas*, Vol. 8, May 2001, pp. 2579–2586.

[26]Vondra, R. J., and Thomassen, K. I., "Flight Qualified Pulsed Electric Thruster for Satellite Control," *Journal of Spacecraft and Rockets*, Vol. 11, No. 9, 1974, pp. 613–617.

[27]Ebert, W. L., Kowal, S. J., and Sloan, R. F., "Operational Nova Spacecraft Teflon Pulsed Plasma Thruster System," AIAA Paper 89-2497, July 1989.

[28]Saccoccia, G., Gonzalez del Amo, J., and Estublier, D., "Electric Propulsion: A Key Technology for Space Missions in the New Millennium," *ESA Bulletin*, No. 101, Feb. 2000, pp. 62–71.

[29]Tajmar, M., Steiger, W., and Genovese, A., "Experimental Characterization of Indium FEEP Microthrusters," *NASA Advanced Propulsion Workshop*, Marshall Space Flight Center, Huntsville, AL, April 2001.

[30]LISA Science Working Group, *LISA Mission Concept Study: Laser Interferometer Space Antenna for the Detection and Observation of Gravitational Waves*, edited by W. M. Folkner, P. L. Bender, and R. T. Stebbins, NASA Jet Propulsion Lab., JPL Publ. 97-16, California Inst. of Technology, Pasadena, CA, 1997.

[31]Ziemer, J. K., and Choueiri, E. Y., "Performance and Erosion Measurements of Gas-Fed Pulsed Plasma Thrusters at NASA Jet Propulsion Laboratory," Electronic Propulsion and Plasma Dynamics Lab., Rept. EPPDyL-JPL99a, Princeton Univ., Princeton, NJ, March 1999.

[32]Blandino, J., Birx, D., Ziemer, J. K., and Choueiri, E. Y., "Performance and Erosion Measurements of the PT8 Gas-Fed Pulsed Plasma Thruster," Electronic Propulsion and Plasma Dynamics Lab., Rept. EPPDyL-JPL99b, Princeton Univ., Princeton, NJ, Aug. 1999.

[33]Morring, F., Jr., "EO-1 Satellite Demonstrates Autonomous Formation Flying," *Aviation Week and Space Technology*, Vol. 154, No. 21, May 2001, pp. 46, 48, 49.

[34]Hoyt, R., "Tether Systems for Satellite Deployment and Disposal," International Astronautical Federation, IAF Paper 00-S.6.04, Oct. 2000.

[35]Carroll, J. A., "SEDS Deployer Design and Flight Performance," AIAA Paper 93-4764, 1993.

[36]DeCou, A. B., "Attitude and Tether Vibration Control in Spinning Tethered Triangles for Orbiting Interferometry," *Journal of the Astronautical Sciences*, Vol. 41, No. 3, 1993, pp. 373–398.

[37]Lakshmanan, P. K., Modi, V. J., and Misra, A. K., "Dynamics and Control of the Tethered Satellite System in the Presence of Offset," *Acta Astronautica*, Vol. 19, No. 2, 1989, pp. 145–160.

[38]Zhu, R., Misra, A. K., and Modi, V. J., "Dynamics and Control of Coupled Orbital and Libration Motion of Tethered Satellite Systems," *Journal of the Astronautical Sciences*, Vol. 42, No. 3, 1994, pp. 319–342.

[39]Cosmo, M. L., and Lorenzini, E. C. (eds.), *Tethers in Space Handbook*, 3rd ed., Smithsonian Astrophysical Observatory, Cambridge, MA, 1997, pp. 1–33, 101–110, and 137–164.

[40]Hoyt, R. P., and Forward, R. L., "The Hoytether: A Failsafe Multiline Space Tether Structure," *Proceedings of the Tether Technology Interchange Meeting*, NASA TR 19980202368, 1997.

[41]Forward, R. L., and Hoyt, R. P., "Failsafe Multiline Hoytether Lifetimes," AIAA Paper 95-2890, July 1995.

[42]Beletsky, V. V., and Levin, E. M., *Dynamics of Space Tether Systems*, Univelt, San Diego, CA, 1993, pp. 339–442.

J. A. Martin
Associate Editor